iScience

CellPress
OPEN ACCESS

Article

IGF2BP2-Shox2 axis regulates hippocampal-neuronal senescence to alleviate microgravity-induced recognition disturbance

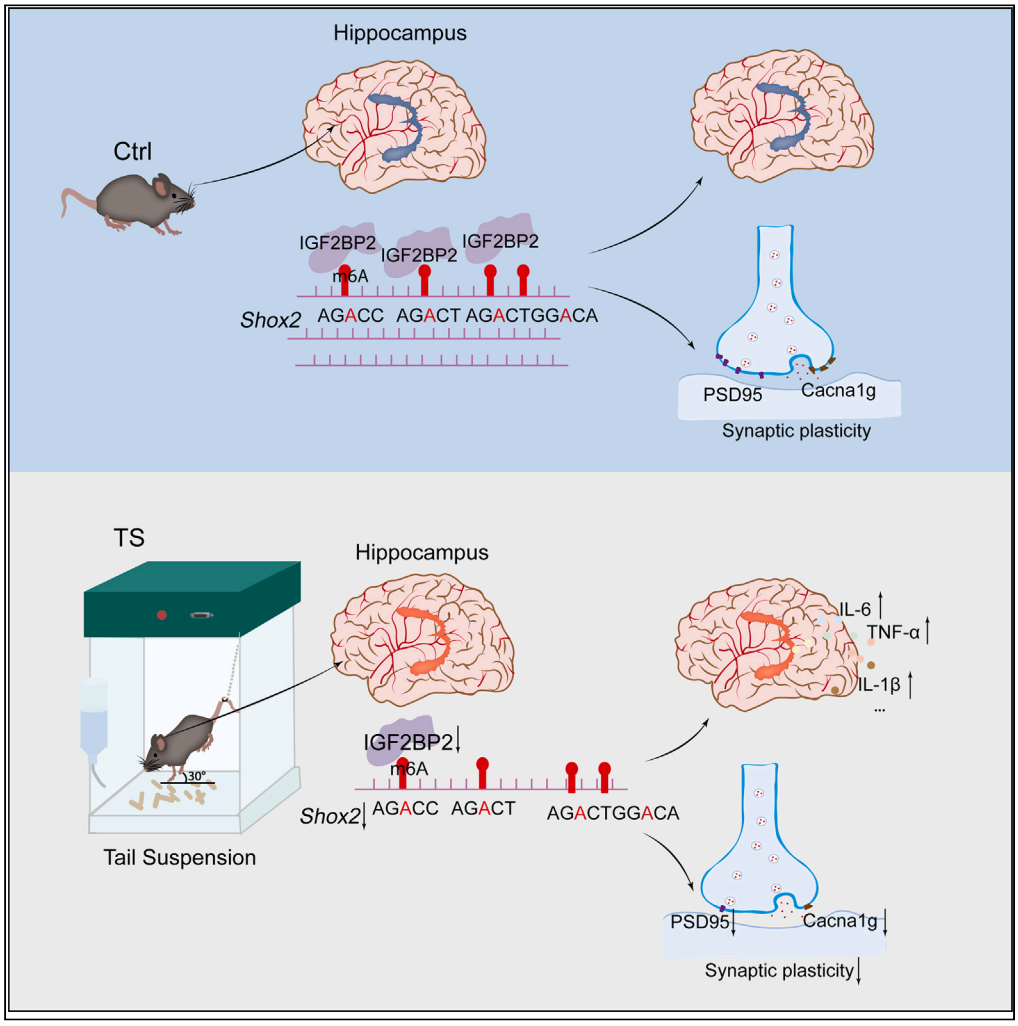

Yujie Zhao, Guohua Ji, Sihai Zhou, ..., Xiaopeng Li, Bo Song, Lina Qu

lixiaopeng_acc@163.com (X.L.)
bosong@dmu.edu.cn (B.S.)
linaqu@263.net (L.Q.)

Highlights

TS mice showed neuronal senescence in the hippocampus

Simulated microgravity induced m6A changes

IGF2BP2-Shox2 axis regulated microgravity-induced neuronal aging and cognitive decline

Zhao et al., iScience *27*, 109917
June 21, 2024
https://doi.org/10.1016/j.isci.2024.109917

iScience

CellPress
OPEN ACCESS

Article

IGF2BP2-Shox2 axis regulates hippocampal-neuronal senescence to alleviate microgravity-induced recognition disturbance

Yujie Zhao,[1,2,4] Guohua Ji,[1,4] Sihai Zhou,[1,2] Shiou Cai,[1,2] Kai Li,[1] Wanyu Zhang,[3] Chuanjie Zhang,[1] Na Yan,[1] Shuhui Zhang,[1] Xiaopeng Li,[1,*] Bo Song,[2,*] and Lina Qu[1,5,*]

SUMMARY

During space travel, microgravity leads to disturbances in cognitive function, while the underlying mechanism is still unclear. Simulated microgravity mice showed neuronal age-like changes in the hippocampus of our study. In the context of microgravity, we discovered m6A modification reshapes in the hippocampal region. When paired with RNA-seq and MeRIP-seq, *Shox2* was found to be a powerful regulator in hippocampal neuron that respondes to microgravity. Decreased expression of senescence-associated secretory phenotype factors and improved genes related to synapses led to the restoration of memory function in the hippocampus upon increased expression of Shox2. Moreover, we discovered that IGF2BP2 was required for the m6A modification of the *Shox2*, and overexpressed IGF2BP2 in the hippocampus protected against both neuronal senescence and learning and memory decline caused by loss of gravity. Accordingly, our research identified the hippocampal IGF2BP2-Shox2 axis as a possible therapeutic approach to maintaining cognitive function during space travel.

INTRODUCTION

Cognitive dysfunction poses an enormous challenge for astronauts during space exploration, thereby emphasizing the imperative for further research in this field.[1–4] Neuroinflammation,[5] increased oxidative stress[6] and the decreased survival of new neurons[7] have been observed in the brain under microgravity conditions. According to the NASA Twins Study, cognitive function can decline following spaceflight and last for up to six months.[8] Therefore, understanding the effects of the microgravity environment on astronauts' cognitive function is key to guaranteeing the success of missions. Given these negative effects, it is imperative to identify the molecular mechanisms of cognitive function and then create innovative preventive and therapeutic approaches to address the issue of cognitive dysfunction.

Neural senescence is a key marker of cognitive impairment in many neurodegenerative disorders.[9,10] Low-grade inflammation is a major driver of aging-related injuries and diseases.[11,12] In Alzheimer's disease (AD), neuroinflammation contributes as much or more to the pathogenesis than plaques and tangles themselves, and inflammation is substantially involved early in the disease's pathogenesis.[13] Senescent cells, during accumulation, can contribute to the progression of neurodegenerative diseases through their abnormal inflammatory secretion set, known as senescence-associated secretory phenotype (SASP).[14] The fact that inflammatory factors such as interleukin-1 alpha (IL-1α), interleukin-1 beta (IL-1β), and interleukin-1 receptor antagonist (IL-1ra) increase in astronauts during a specific flight mission,[15] coupled with stress-induced cortisol elevation and insulin resistance, resembles classic aging-like phenomena.[16] Multiple data suggest that IL-1α and IL-1β, the senescence-associated secretory phenotype (SASP) factors, are involved in long time potentiation (LTP) induction and maintenance as well as memory and learning processes.[17–20] TNF also plays a necessary and constitutive role in regulating AMPAR membrane insertion and altering synaptic strength.[21,22] Tzeng et al. confirmed that IL18-deficient AD mice exhibit increased excitatory synaptic protein, spine density, and basal excitatory synaptic transmission.[23] However, it is still unclear whether astronauts will experience age-like changes in neurons while in space, as well as the specific mechanism linking neuroinflammation to cognitive dysfunction in microgravity. Further research is needed to elucidate these complex interactions and their potential implications especially for long-duration space travel.

Changes in RNA N6-methyladenosine (m6A) methylation patterns occurred in the brain of neurodegenerative mice and in the hippocampus of aging mice.[24,25] m6A can govern the plasticity of hippocampal synapses, thereby influencing neuronal transmission and synaptic strength.[26–29] Deficiency of the m6A writer METTL3 enhanced cognitive function in mouse models of amyloid (Aβ)-induced Alzheimer's

[1]State Key Laboratory of Space Medicine, China Astronaut Research and Training Center, Beijing, China
[2]Department of Pathology and Forensics, Dalian Medical University, Dalian, China
[3]Basic Medical Sciences, Capital Medical University School, Beijing, China
[4]These authors contributed equally
[5]Lead contact
*Correspondence: lixiaopeng_acc@163.com (X.L.), bosong@dmu.edu.cn (B.S.), linaqu@263.net (L.Q.)
https://doi.org/10.1016/j.isci.2024.109917

disease (AD).[30] And deficits in learning and memory were observed in mice with m6A reader YTHDF1 gene deletion, along with compromised synaptic transmission and long-term enhancement in the hippocampus.[29] m6A has also been shown to regulate processes associated with SASP. According to reports, m6A can regulate the expression of CDKN2B, and knocking down METTL3 can restore the SASP.[31] Liu et al. also demonstrated that METTL3 and METTL14 are necessary for SASP.[32] Mutant METTL14 leads to significant enrichment of SASP-related pathways such as inflammatory cytokines and NF-κB pathways. All of this confirmed that m6A plays an important role in regulating cognitive function and senescence, which motived us to hypothesize that m6A plays a role in modulating learning and memory in microgravity.

Here, we showed that the hippocampus of mice exhibited an augmented secretion of age-related secretory phenotype-associated factors, increased expression of genes associated with aging, and a larger area positive for β-galactosidase (β-Gal) staining in the microgravity environment. The hippocampus undergoes m6A remodeling, which has been linked to these changes. Disruption of m6A modification in Short Stature Homobox2 (Shox2) can lead to deficits in synaptic plasticity and a phenotype similar to senescent secretion. The modifications in the *Shox2* m6A modification required insulin growth factor 2 mRNA binding protein 2 (IGF2BP2), which is a m6A reader. Furthermore, it has been shown that overexpressed IGF2BP2 and Shox2 in the hippocampus can lessen the phenotype similar to senescent secretion brought on by microgravity, as well as the decline in learning and memory. This work laid the foundation for future investigations into the mechanisms underlying cognitive function.

RESULTS

The hippocampus neurons of the 42-day tail-suspension mice showed accelerated senescence

Given the current trend in manned spaceflight toward long-duration missions, we designed a longer-time tail suspension (TS) on mice than that of reported.[33] Morris water maze (MWM) and novel object recognition (NOR) tests were used to assess the learning and memory abilities of mice.[34,35] After 5-day MWM training, TS mice made little progress in escape latency and took more time to locate the hidden platform compared to the control group. Also, the routes of mice in the TS group were disorganized and chaotic, indicating prolonged latency (Figure S1A). In the spatial probe tests on the sixth day, the number of crossings (Figure S1C), swimming distance (Figure S1D) and time in the target quadrant (Figure S1E), as well as the percentage of swimming distance and time (Figures S1F and S1G) in the target quadrant, were significantly reduced in the TS group, with no difference in swimming speed between two groups (Figure S1B). As for the non-spatial learning and memory processes, NOR test data indicated TS mice spent less time in exploring the novel object (Figure S1H) and the novel location (Figure S1I) compared to control group. These behavioral tests implied that TS mice have compromised learning and memory capacities. We then measured the expressions of molecules associated with learning and memory in the mice hippocampus. Likewise, protein levels of phosphorylated-cAMP-response element binding protein (*p*-CREB) (Figure S1J), the voltage-dependent T-type calcium channel subunit alpha-1G (Cacna1g), postsynaptic density protein 95 (PSD95) and brain derived neurotrophic factor (BDNF) were decreased in the TS mice hippocampus (Figure S1K).

To investigate the molecular mechanism, we first performed RNA-seq analysis on two different groups of hippocampi. Totally, 224 upregulated and 103 downregulated genes were identified between the TS and control group (Figure 1A). Interestingly, we found several genes related to senescence and neuronal function such as *Cdkn1a* (encoding *p21*), *Klotho* (*KL*) and *Fos*, which showed significant changes, indicating the likely involvement of neural senescence (Figures 1B and 1C). To verify this hypothesis, senescence-related genes such as *p16*, *p21*, and *p38* were detected using RT-qPCR and their expressions were found to be increased significantly in the hippocampus of TS mice (Figure 1D). Notably, a larger dye-positive area of β-galactosidase (β-Gal), a classical aging biomarker, was observed in TS mice hippocampus neurons (Figure 1E). In addition, we observed augmented secretion of SASP factors, including IL-6, IL-1β, and TNF-α (Figure 1F). We further performed the Nissl staining assay and found that the number of Nissl-body was decreased in the CA1 and CA3 regions of the TS group hippocampus (Figure 1G).

Taken together, these findings suggested mice under simulated microgravity condition exhibited impaired learning and memory abilities and prompted neural senescence in the hippocampus.

The m6A landscape in the hippocampus of tail suspension mice was changed

m6A modification is one of the key processes relative to mRNA regulation and has been reported to play a role in neurodegenerative diseases, so we wondered if microgravity disturbs neural m6A modification. First, we stained the hippocampal tissue with m6A antibody and found that the level of m6A in hippocampal neurons decreased significantly under simulated microgravity (Figure 2A). MeRIP-seq analysis of the m6A epigenetic transcriptome was then carried out. The analysis showed that there were 1371 differentially methylated peaks (DMPs), of which 548 were upregulated and 823 were downregulated in the TS mice hippocampus (Figure 2B). Several genes related to neuroimmunology and neurodegenerative diseases such as *Syk*, *Mmp28*, *Il16*, and *Camk2d* enriched functional terms that "Response to stimulus," indicating that m6A is involved in neuronal function under space stress (Figure 2C). Also, the *Cdkn1a* was involved in the "Endocrine system," and *Cacna1e*, *Camk2d* were involved in "Endocrine and metabolic disease" (Figure 2D). Figure 2E showed the distribution of the peaks, which displays a comparable m6A density enrichment under all conditions.

RT-qPCR was further used to detect the expressions of m6A writers (*Mettl3*, *Mettl14*, *Wtap*, *Kiaa1249*, *Mettl16*, and *Rbm15*), erasers (*Fto* and *Alkbh5*), and m6A readers (*Hnrnpc*, *Ythdf1/2/3* and *Igf2bp1/2/3*) in the hippocampal tissues of mice. The results showed that the simulated microgravity mice contained significantly fewer mRNA level of *Mettl3*, *Mettl14*, and *Igf2bp2* (Figures 2F and 2G). And western blot

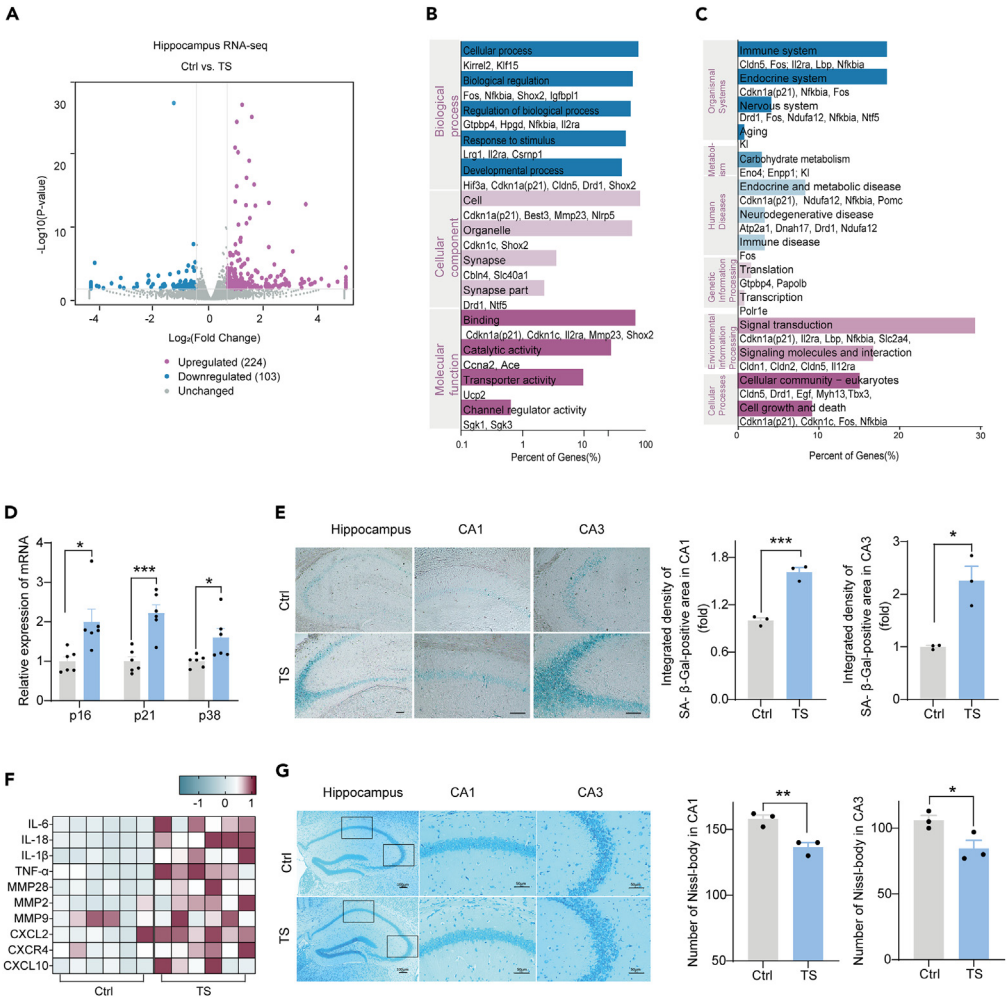

Figure 1. 42 days of simulated microgravity impaired mice learning and memory capability and exhibited a senescence phenotype

(A) Volcano plots of the differentially expressed genes (DEGs) between control and TS mice hippocampus.

(B) Gene Ontology (GO) enrichment analysis of DEGs in control and TS mice.

(C) KEGG pathway analysis of DEGs in control and TS mice.

(D) RT–qPCR analysis of the relative expression of *p16*, *p21* and *p38* in mice hippocampus ($n = 6$ per group).

(E) Representative images of SA-β-Gal-positive cells in mice hippocampus. Scale bars: 100 μm (main images) and 50 μm (magnified images).

(F) The heatmap of mRNA levels of senescence-associated secretory phenotype (SASP) factors in the mice hippocampus ($n = 6$ per group). SASP factors include the inflammation factors of *Il-6*, *Il-18*, *Il-1β*, *Tnf-α*; matrix metalloproteinase of *Mmp2, Mmp9, Mmp28*; and chemokines of *Cxcl2*, *Cxcr4* and *Cxcl10*.

(G) Nissl staining of hippocampus of control and TS group and statistical analysis of CA1 and CA3 in hippocampus ($n = 3$ for each group). (*$p < 0.05$, **$p < 0.01$, ***$p < 0.001$).

confirmed the decreased expressions of IGF2BP2 in the TS group (Figures S2A and S2B). Thus, our results demonstrated that simulated microgravity may induce neural m6A modification in the hippocampus.

Identification of short stature homeobox 2 as a hub gene related to impaired learning and memory under simulated microgravity environment

In order to investigate the possible relationship between m6A molecular fluctuations and the heightened vulnerability to cognitive function during microgravity stimulation, we combined the data from the DEGs and DMPs analyses and discovered a total of 31 genes overlapped (Figure 3A). We also confirmed their mRNA levels in the hippocampal tissues using RT-qPCR (Figures S3A–S3D). Notably, *Shox2*, a highly hypomethylated and downregulated protein in the TS mice hippocampus drew our attention and further verification showed that the mRNA and protein levels of Shox2 were both significantly decreased (Figures 3B and 3C). As shown in Figure 3D, the m6A modification level of *Shox2* mRNA in the hippocampus of the TS group was also decreased using MeRIP-qPCR analysis. To test whether Shox2 was involved in microgravity-induced aging-like changes, we first treated HT22 cells with D-gal and found this treatment led to lower levels

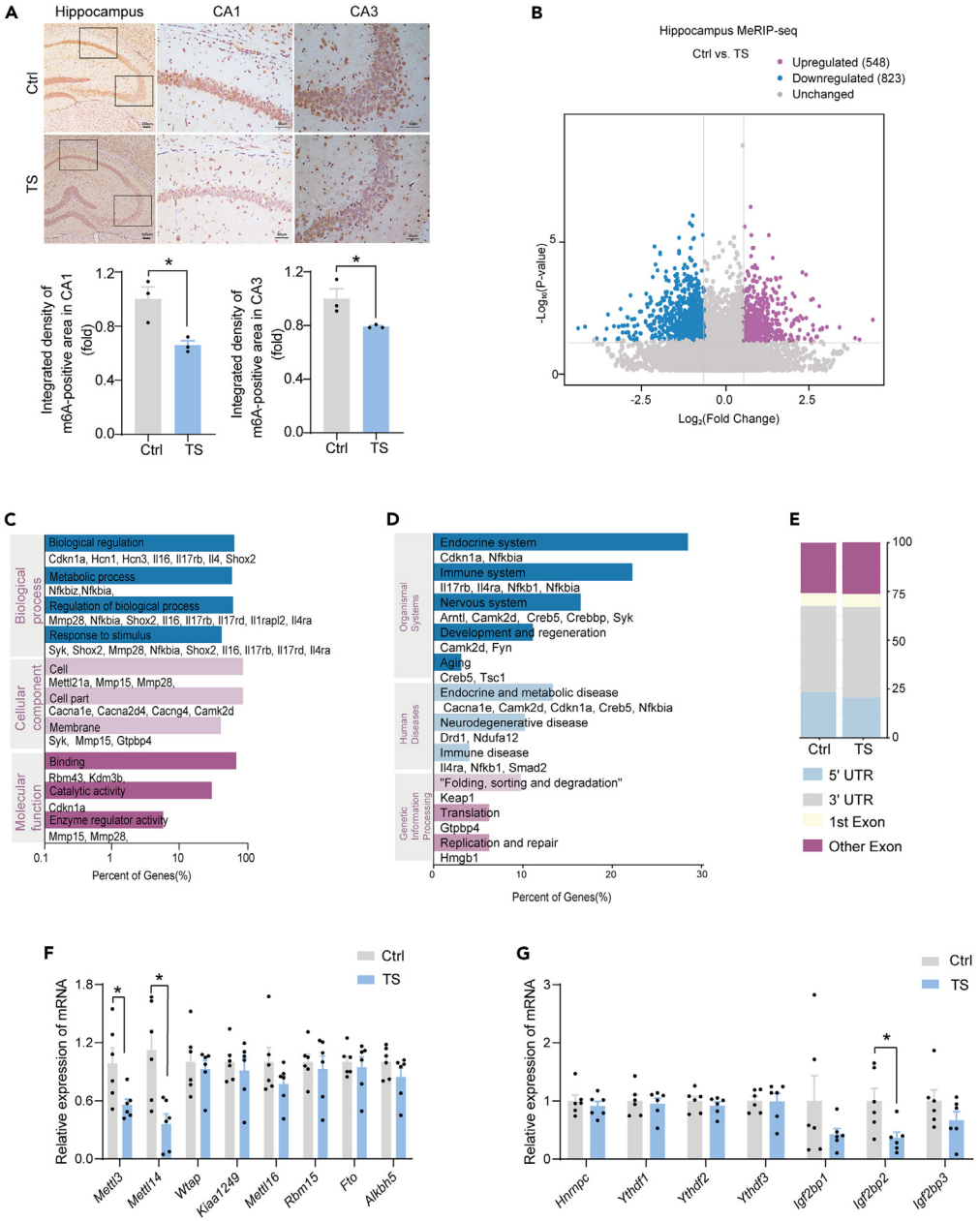

Figure 2. The m6A landscape in the hippocampus of TS mice was changed

(A) The m6A staining in the hippocampus of TS mice showed decreased in m6A levels. The representative image was shown. Scale bars: 100 μm (main images) and 50 μm (magnified images).

(B) Volcano plots of the differentially methylated peaks (DMPs) between control and TS mice.

(C) Gene Ontology (GO) enrichment analysis of differentially expressed genes in control and TS mice.

(D) KEGG pathway analysis of differentially expressed genes in control and TS mice.

(E) Distribution analysis of differentially m6A peaks between control and TS mice along the four transcript segments: 5'UTR, 3'UTR, 1st exon and other exon. Data were shown as percentage of total differential peaks.

(F) RT-qPCR of m6A writers and erasers mRNA levels in the hippocampal tissues of control and TS mice ($n = 6$ per group). (G) RT-qPCR of m6A readers mRNA levels in the hippocampal tissues of control and TS mice ($n = 6$ per group). (*$p < 0.05$, **$p < 0.01$, ***$p < 0.001$).

of *Shox2* mRNA (Figure 3E). RNA-seq analysis following the application of siRNA (*si-Shox2*) in HT22 cells (Figure S4A), indicated that 136 additional genes were downregulated in addition to the initial downregulated genes (Figure 3F). GO and KEGG analyses of these genes were shown in Figures 3G and 3H. Analyses of 54 up-regulated genes were shown in Figures S4B and S4C. The up-regulated gene pathway

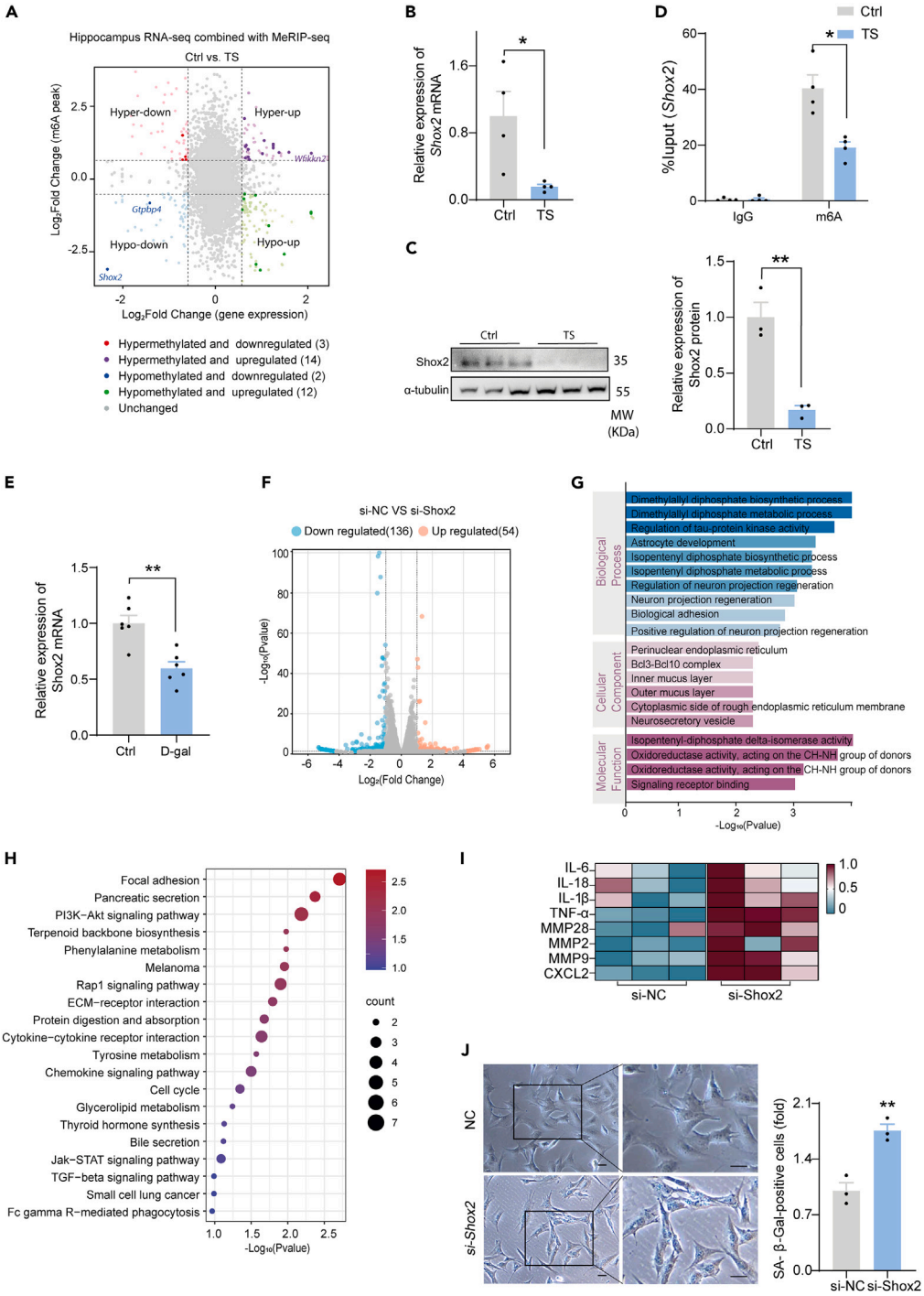

Figure 3. Shox2 expression was downregulated in the hippocampus of TS mice

(A) Differential methylation peaks and differential expressed genes were jointly analyzed, and a four-dimensional quadrant map was generated. Hyper-up: Compared to the hippocampal tissue of the control mice, the TS group showed hypermethylated in genes with upregulated. Hypo-up: hypomethylated genes with upregulated; Hypo-down: hypomethylated genes with downregulated; Hypo-down: hypomethylated genes with downregulated. Representative genes have been labeled on the chart.

(B) The mRNA level of Shox2 in the hippocampus of TS group was significantly decreased (n = 4 per group).

(C) Western blot to assess the Shox2 protein level in TS mice hippocampus. The protein level of Shox2 was significantly decreased in TS group (n = 3 per group).

Figure 3. *Continued*

(D) The m6A level of *Shox2* was decreased in the hippocampus of the TS mice. The level of m6A in the hippocampus of TS group was significantly decreased ($n = 4$ per group).

(E) D-gal treated HT22 cells to simulated cell senescence and RT-qPCR detected a decrease in *Shox2* mRNA levels ($n = 6$ per group). (F) The heatmap of SASP factors mRNA levels after *si-Shox2* ($n = 3$ per group).

(G) GO enrichment analysis of downregulated genes after *si-Shox2*. (H) KEGG pathway analysis of downregulated genes after *si-Shox2*. (I) The heatmap of senescence-associated secretory phenotype (SASP) factors mRNA levels in control and *si-Shox2* group ($n = 3$ per group).

(J) SA-β-Gal staining analysis in *si-NC* and *si-Shox2* HT22 cells. Left: representative images. Right: the percentage of SA-β-Gal-positive cells is quantified. Scale bars: 50 μm ($n = 3$ per group). (*$p < 0.05$, **$p < 0.01$, ***$p < 0.001$).

analysis also enriched the immune-related pathway "Macrophage colony stimulating factor receptor binding." Importantly, we found the secretion of SASP factors in HT22 cells was increased when *Shox2* was silenced (Figure 3I). Meanwhile, the dye-positive area of β-galactosidase in cells was elevated significantly in the *si-Shox2* group (Figure 3J). As predicted, we observed a significant decrease in the expression of genes associated with synapses, including *PSD95*, *Hcn1*, and *Cacna1g* following transfection with siRNA (*si-Shox2*) (Figure S4D). In line with the downregulation of the Shox2 protein (Figure S4E), there was a decrease in protein levels of Cacna1g and PSD95 (Figure S4F). The expressions of *SYN*, *Hcn1*, *Cacna1g*, and *Cacna1h* were also upregulated by Shox2 overexpression (Figure S4G), similarly, protein levels of Cacna1g and PSD95 were also upregulated (Figures S4H and S4I). Collectively, m6A modification of Shox2 in the hippocampus of mice might be responsible for impaired learning and memory function as well as neuronal aging under simulated microgravity conditions by downregulating synapse-related genes.

Overexpression of short stature homeobox 2 improved cognitive function and alleviated neural senescence in tail suspension mice

To further verify the impacts of Shox2 expression on the learning and memory of mice, we designed overexpression of *Shox2* recombinant adeno-associated virus (rAAV). The virus was injected into the CA1 region of the hippocampus at two weeks before performing 42-day TS (Figure 4A, upper panel). Shox2 protein level was confirmed in the hippocampal tissues by Western blot (Figure S5A). The escape latency of (TS + OE-Shox2) group was decreased relative to the TS group at the fourth and fifth day (Figure 4A, middle panel). Meanwhile, the movement trajectories of (TS + OE-Shox2) group became more organized compared with the TS group (Figure 4A, lower panel). Even though there was no significant difference in the swimming speed (Figure 4B), we noticed the increased times of target crossing (Figure 4C), swimming distance and time in the target quadrant (Figures 4D and 4E), and percentage of swimming distance and time in the target quadrant (Figures 4F and 4G) in the (TS + OE-Shox2) group compared to the TS group. In the NOR test, mice in the (TS + OE-Shox2) group spent significantly more time exploring the novel object (Figure 4H) and the novel location (Figure 4I) compared to the TS group. Furthermore, both protein and mRNA levels of PSD95 and Cacna1g were elevated in (TS + OE-Shox2) group of mice hippocampus (Figures S5B–S5D). Nissl staining assay demonstrated that the density of Nissl-body was increased in the CA3 region neurons compared with the TS group (Figure S5E). Although there was no obvious improvement in the genes related to aging, Shox2 overexpression led to a decrease secretion of senescence-associated inflammation factors in comparison with the TS group (Figure 4J and 4K). Taken together, our *in vivo* study further proved that Shox2 plays a role in microgravity-induced cognition decline and that overexpression of Shox2 benefits against neural aging in TS mice.

IGF2BP2 mediated perturbation of short stature homeobox 2 deficiency through direct binding to the m6A modification sites

Based on the changes in the m6A modification and mRNA levels of *Shox2*, we wondered which methylation-related enzyme may be involved in the regulation of *Shox2*. Our results showed that IGF2BP2 was decreased in the hippocampal tissues of the TS group at mRNA and protein levels (Figures 2F, 2G, S2A, S2B; 5A). We first examined the relationship between Shox2 and IGF2BP2. Knockdown *Igf2bp2* by siRNA (Figures S6A and S6B) downregulated Shox2 expressions both at mRNA and protein levels (Figures 5B and 5C). *Igf2bp2* overexpression (Figure S6C) upregulated the levels of Shox2 mRNA (Figure 5D) and protein (Figure 5E). The result of RIP-qPCR showed that *Shox2* mRNA expression was significantly increased after incubation with IGF2BP2 antibody (Figure 5F), suggesting that *Shox2* mRNA can be affiliated with IGF2BP2. Secondly, we found four high-confidence m6A modification sites within *Shox2* mRNA utilizing the online tool SRAMP, and the mutant plasmids targeting these four sites were constructed respectively (Figure 5G). Luciferase assay results showed that the luciferase activity was dramatically increased after wild-type *Shox2* plasmid transfection, however, *Shox2*-Mut2, -Mut3, and -Mut4 transfection significantly decreased the luciferase activity (Figure 5H). From two perspectives, we confirmed the direct site-binding relationship of IGF2BP2 and Shox2. As for the character of IGF2BP2 in aging-like changes, we treated HT22 cells with D-gal and found lower levels of IGF2BP2 mRNA (Figure 5I) and protein (Figure 5J). We also found that the secretion of aging-related inflammation was induced (Figure 5K) and the dye-positive area of β-galactosidase increased (Figure 5L) after knocking down IGF2BP2 with siRNA. Additionally, overexpression of IGF2BP2 resulted in elevated mRNA levels of *PSD95* and *Cacna1g*. This overexpression effect was notably suppressed when *Shox2* siRNA was introduced (Figure S6D), and the same effect was shown in protein levels (Figures S6E and S6F). After knocking down *Igf2bp2*, the expressions of synapse-related genes were also decreased (Figure S6G). These data further supported the regulatory role of IGF2BP2 in synapse-related gene expression via Shox2.

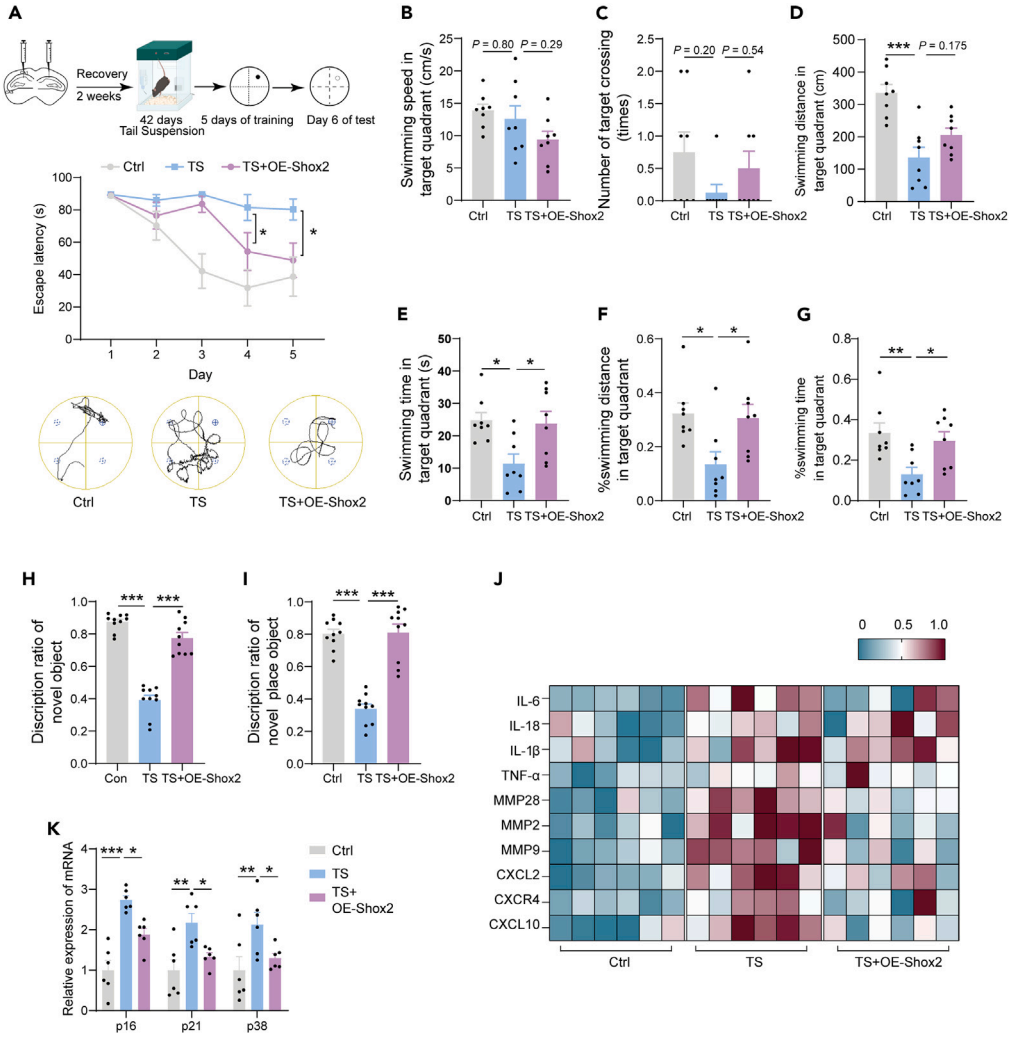

Figure 4. The recovery effect of Shox2 on the learning and memory impairment induced by simulated microgravity

(A) Spatial learning deficits were observed in the Shox2 over expressed mice, TS and the control mice in the Morris Water Maze (MWM) assay (n = 6 per group). The protocol of experiment was shown in the upper panel, the escape latency curve was displayed in the middle panel, and the lower panel was the representative image of the movements of mice in each group at the fifth day.

(B–G) The memory phase in the sixth day of MWM test was shown. Swimming speed in target quadrant (B); number of target crossing (C); swimming distance in target quadrant (D); swimming time in target quadrant (E); ratio of swimming distance in target quadrant (F) and ratio of swimming time in target quadrant (G) (n = 8 per group).

(H and I) Non-spatial learning and memory ability was declined in the TS mice compared with the control mice in the NOR test (n = 10 for each group). New object recognition (H) and new location recognition test (I).

(J) The levels of SASP factors in the hippocampus were reduced when Shox2 overexpressing (n = 6 per group).

(K) The genes related to aging were detected by RT-qPCR (n = 6 for each group). (*p < 0.05, **p < 0.01, ***p < 0.001).

Overexpression of IGF2BP2 improved the cognitive function and alleviated neural senescence in tail suspension mice

Since we defined the m6A reader IGF2BP2 can regulate Shox2 *in vitro*, we next determined the effects of IGF2BP2 in the cognitive function and neuronal senescence *in vivo*. We designed IGF2BP2-rAAV and injected virus into the CA1 region of the hippocampus of at two weeks before performing 42-day TS, the procedures were shown in the upper panel of Figure 6A. IGF2BP2 was verified to be significantly overexpressed (Figure S7A). The escape latency of the MWM test was found to be rescued after IGF2BP2 overexpression (Figure 6A, middle panel), and the movement trajectories became organized compared with the TS group (Figure 6A, lower panel). In the day 6 of the MWM test, IGF2BP2-rAAV injection into the hippocampus showed an improved effect on the memory of the TS mice (Figures 6B–6G). The ability to learn and remember new things in the NOR/OLRT test was also improved in the IGF2BP2-rAAV injection group (Figures 6H and 6I). After the behavioral experiment, we detected age- and SASP-related gene expressions. We found that *p16*, *p21* and *p38* mRNA levels showed a decreased tendency, and the reduction of *p21* mRNA reached the significance (Figure 6J). The mRNAs of SASP related genes in overexpressed-IGF2BP2

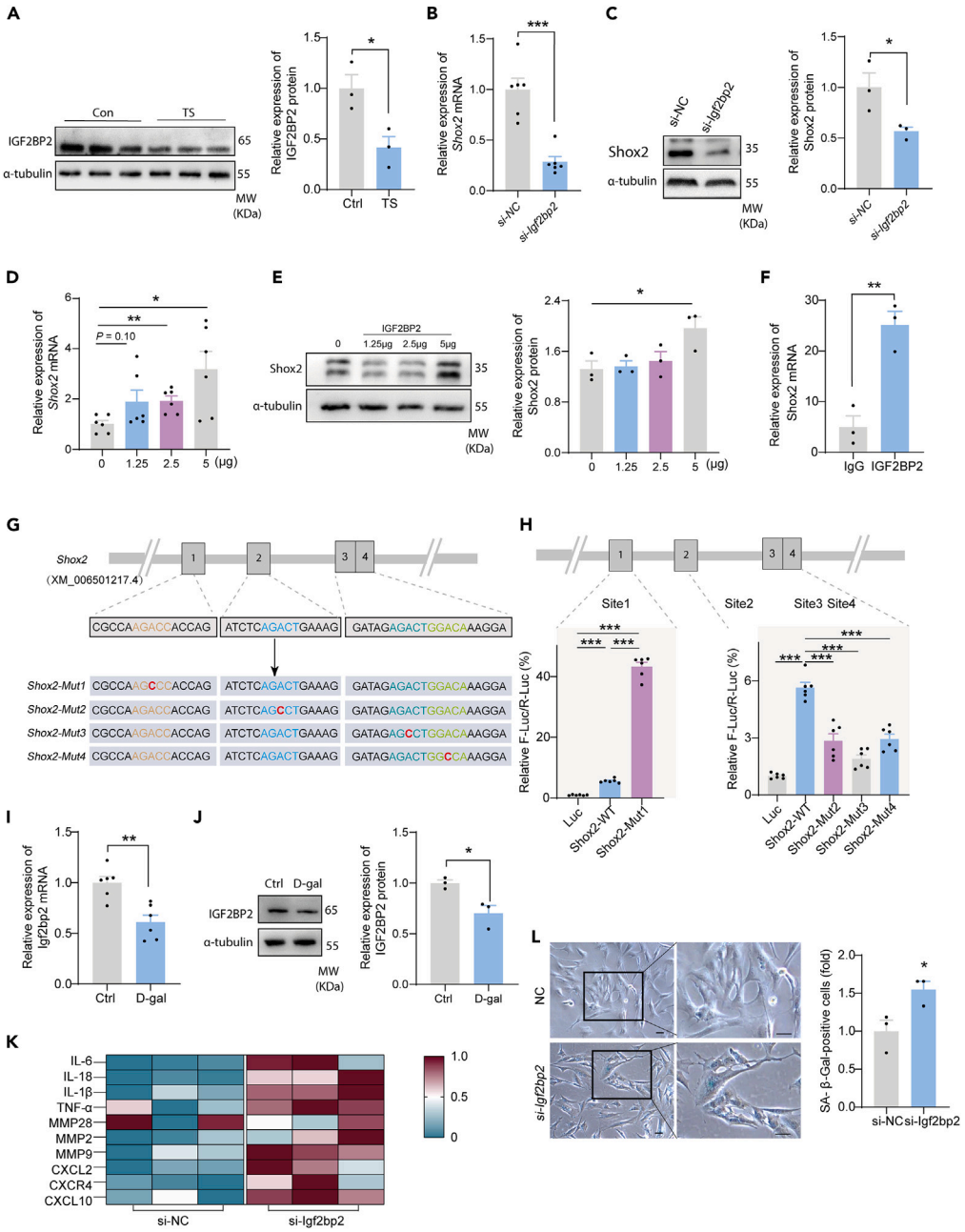

Figure 5. The m6A reader IGF2BP2 recognizes and binds to the *Shox2* m6A modification sites

(A) The protein expression of IGF2BP2 was decreased in TS mice hippocampus (n = 3 for each group).

(B) The mRNA expression of *Shox2* was decreased after *Igf2bp2* knockdown (n = 6 for each group).

(C) The protein expression of Shox2 was also decreased after *Igf2bp2* knockdown (n = 3 for each group).

(D) The mRNA expression of *Shox2* was increased after Igf2bp2 over expressed (n = 6 for each group).

(E) The protein expression of Shox2 was also increased after *Igf2bp2* overexpressed (n = 3 for each group).

(F) RIP-qPCR detected *Shox2* as a binding mRNA molecule downstream of IGF2BP2 (n = 3 for each group).

(G) Predicted binding sites of *Shox2* with IGF2BP2 and the constructed mutant plasmids at four sites.

(H) Luciferase analysis showed the binding sites of *Shox2* with IGF2BP2 were 2, 3 and 4 in HT22 cells (n = 6 for each group).

(I) the *Igf2bp2* mRNA level was reduced after D-gal treatment in HT22 cells (n = 6 for each group).

(J) D-gal treated induced decreased IGF2BP2 protein expression in HT22 cells (n = 3 for each group).

(K) The heatmap of senescence-associated secretory phenotype (SASP) factors mRNA levels in control and *si-Igf2bp2* group (n = 3 per group). (L) SA-β-Gal staining analysis in *si-NC* and *si-Igf2bp2* HT22 cells. Left: representative images. Right: the percentage of SA-β-Gal-positive cells is quantified. Scale bars: 50 μm (n = 3 per group). (*p < 0.05, **p < 0.01, ***p < 0.001).

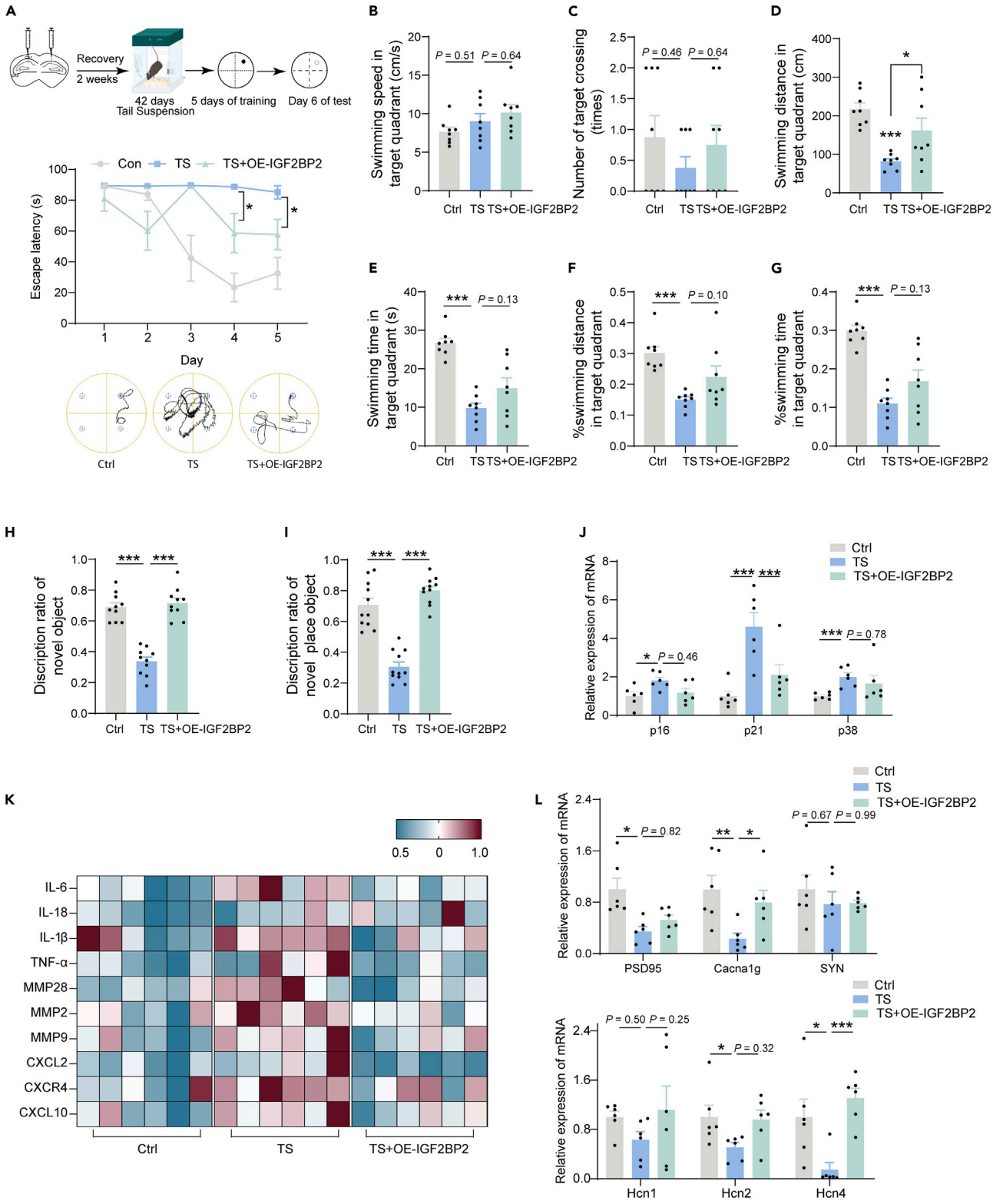
A
Recovery
2 weeks
42 days
Tail Suspension
5 days of training
Day 6 of test
Con
TS
TS+OE-IGF2BP2
Escape latency (s)
Day
Ctrl
TS
TS+OE-IGF2BP2
B
Swimming speed in target quadrant (cm/s)
P = 0.51
P = 0.64
C
Number of target crossing (times)
P = 0.46
P = 0.64
D
Swimming distance in target quadrant (cm)
E
Swimming time in target quadrant (s)
P = 0.13
F
%swimming distance in target quadrant
P = 0.10
G
%swimming time in target quadrant
P = 0.13
H
Discription ratio of novel object
I
Discription ratio of novel place object
J
Relative expression of mRNA
p16
p21
p38
P = 0.46
P = 0.78
K
0.5
0
1.0
IL-6
IL-18
IL-1β
TNF-α
MMP28
MMP2
MMP9
CXCL2
CXCR4
CXCL10
L
PSD95
Cacna1g
SYN
P = 0.82
P = 0.67
P = 0.99
Hcn1
Hcn2
Hcn4
P = 0.50
P = 0.25
P = 0.32

Figure 6. The rescuable effect of IGF2BP2 on the learning and memory function decline induced by simulated microgravity

(A) Spatial learning deficits was observed in the IGF2BP2 over expressed mice, TS and the control mice in the MWM assay (n = 5 per group). The protocol of experiment was shown in the upper panel, the escape latency curve was displayed in the middle panel, and the lower panel was the representative image of the movements of mice in each group at the fifth day.

(B–G) The memory phase in the sixth day of MWM test was shown. Swimming speed in target quadrant (B); number of target crossing (C); swimming distance in target quadrant (D); swimming time in target quadrant (E); ratio of swimming distance in target quadrant (F) and ratio of swimming time in target quadrant (G) (n = 8 per group).

(H and I) Non-spatial learning and memory ability was declined in the TS mice compared with the control mice in the NOR test (n = 10 for each group). New object recognition (H) and new location recognition test (I).

(J) The genes related to aging were detected by RT-qPCR (n = 6 for each group).

(K) The mRNA levels of SASP factors in the hippocampus were reduced when IGF2BP2 overexpressing (n = 6 per group).

(L) The synaptic-related genes were detected by RT-qPCR (n = 6 for each group). (*p < 0.05, **p < 0.01, ***p < 0.001).

(OE-IGF2BP2) virus injection group were reduced as well (Figure 6K). Meanwhile, the mRNA levels of *Cacna1g* and *Hcn4* were increased (Figure 6L). Nissl staining assay showed that the density of Nissl-body was increased in the CA1 and CA3 regions neurons compared with the TS group (Figure S7B). Taken together, our findings revealed that IGF2BP2 could improve the learning and memory ability and inhibit the release of inflammatory factors associated with the aging phenotype in TS mice.

DISCUSSION

Previous studies have demonstrated reduced learning and memory in mice in simulated microgravity environments,[36] and our two tests MWM and NOR have demonstrated this. Then, to our surprise, we discovered that 42 days of microgravity stimulation resulted in neural senescence in mice. This showed up as: 1. Exhibited an augmented secretion of age-related secretory phenotype-associated factors; 2. Increased expression of genes associated with aging; 3. A larger area positive for β-galactosidase (β-Gal) staining. Moreover, dysregulation of m6A modification in simulated microgravity upsets patterns of gene expression and results in cognitive deficits. According to our findings, *Shox2* plays a crucial regulatory role in this process by modifying m6A. *Shox2* interacts with IGF2BP2, one of the m6A readers, to promote the recruitment of downstream effector proteins such as PSD95 and Cacna1g. When Shox2 and IGF2BP2 levels are lowered, inflammatory factors linked to aging secretion phenotypes release. After overexpression of these two molecules *in vivo*, the senescence of hippocampus neurons are decreased. Thus, our findings imply that the IGF2BP2-Shox2 axis may hold great promise for comprehending the molecular processes involved in learning and memory.

Shox2 is an essential transcription factor of heart development, nervous system function, and embryonic development.[37–39] It has been discovered to be crucial in controlling the development and transmission of synapses and ion channels, such as *HCN4*, *HCN1*, and *CaV1.3*.[40–42] We have further elucidated this process in the nervous system by finding that Shox2 regulates the expression of genes associated with synapses. Our study further found that Shox2 regulates the neuronal senescence process. Age-related sinoatrial node dysfunction (SND) down-regulates Shox2 expression, leading to pacemaker associated ion channel dysfunction.[43] Shox2 also has been found to play an important role in anti-aging pharmacology study.[44] Anti-aging drugs improve the function of T-type calcium ion channels through *Shox2* and *Cacna1g*, which is also consistent with our study.

The m6A modification regulation of aging-related inflammation has drawn a lot of attention in recent years. The loss of *Mettl3* suppresses the inflammatory response induced by lipopolysaccharide (LPS). This in turn inhibits the NF-κB and MAPK signaling pathways, thereby suppressing the inflammatory response.[45] More specifically, by controlling the levels of pro-inflammatory cytokines such as TNF-α, m6A can control the inflammation under METTL3 modification.[46] This implies that aging-related inflammation may be mediated by m6A. The emergence of the inflammation associated with neuronal aging is also caused by IGF2BP2 knockdown, as our study also demonstrated. The following reports also further confirmed that inflammatory factors can further affect synaptic plasticity. Cytokines in SASP such as IL-1β and IL-18 are associated with synaptic plasticity and glutamatergic synaptic activity.[47,48] TNF-α has been implicated in the regulation of synaptic homeostasis.[49] These inflammatory cytokines further affected cognitive function.

Mice exposed to simulated microgravity had altered levels of m6A modification-related enzymes. We screened 15 methylation-related enzymes and found that the IGF2BP family (IGF2BP1, IGF2BP2, and IGF2BP3), in particular, showed more noticeable alterations. Only IGF2BP2 mRNA and protein levels were reduced simultaneously (Figures 2F, 2G; 5A, S2A and S2B), which was consistent with the change of Shox2. Meanwhile, Xiao et al.'s RIP-sequence results of IGF2BP2 also confirmed that Shox2 is its downstream molecule.[50] A specific role for IGF2BP2 in learning and memory has been suggested. IGF2BP2 interacts with mRNA linked to axon guidance and shows notable enrichment in the developing axon bundle.[51] A genetic association study of metabolic syndrome and metabolism-related traits in a Chinese elderly population also explains the association between IGF2BP2 and the symptoms manifested in aging.[52] This also further confirmed our results that IGF2BP2 is involved in the regulation of neural senescence processand offered more proof that IGF2BP2 and Shox2 work together to control synaptic plasticity and are involved in learning and memory functions. Interestingly, we found the first mutated m6A modification site resulted in a significant increase in the binding affinity of IGF2BP2 to Shox2 for above 40 times. We hypothesize that spatial conformation or other factors could be responsible for the notable increase in binding affinity, which would require additional research into the underlying molecular mechanisms.

In conclusion, our research revealed that the IGF2BP2-Shox2 axis is a hitherto unidentified molecular pathway that controls memory and learning as well as the neuronal senescence. Of these, the N6-methyladenosine of *Shox2*, which is controlled by IGF2BP2, is probably a crucial

molecular switch. This study provides evidence that N6-Methyladenosine plays a role in learning and memory in simulated microgravity environments. Shox2 is necessary for normal neuronal development,[53] and IGF2BP2 also plays a key role in neurodegenerative diseases.[54] Therefore, the IGF2BP2-Shox2 axis, which mediates neuronal aging in microgravity may also play an important role in these diseases and become an important target for treatment. To fully understand the neural circuits involved in the modification of the IGF2BP2-Shox2 axis in other neurological disease models, more research is necessary.

Limitations of the study

This experiment only detected the crucial role of the IGF2BP2-Shox2 axis in spatial learning and memory under a simulated microgravity environment, without exploring its involvement in other neurodegenerative diseases or natural aging models. Therefore, further experimental verification is imperative. Additionally, further research is warranted to investigate the regulation of the m6A modification process of Shox2 by other m6A-regulating enzymes. Moreover, given the intricacies of the space environment, we cannot ascertain whether other environmental factors, such as magnetic fields, stress, radiation, and the like, also impact the learning and memory process.

STAR★METHODS

Detailed methods are provided in the online version of this paper and include the following:

- KEY RESOURCES TABLE
- RESOURCE AVAILABILITY
  - Lead contact
  - Materials availability
  - Data and code availability
- EXPERIMENTAL MODEL AND SUBJECT DETAILS
- METHOD DETAILS
  - Tail suspension
  - Morris water maze test
  - Novel object recognition (NOR)/object location recognition test (OLRT)
  - Stereotaxic injection into the hippocampus
  - Western blotting analysis
  - Nissl's staining
  - RT-PCR and RT-qPCR
  - Vector construction and cell transfection
  - D-gal treat cells
  - Senescence-associated β-galactosidase stain (SA-β-gal stain)
  - Immunohistochemistry (IHC)
  - MeRIP-qPCR
  - MeRIP-seq data analysis
  - RNA immunoprecipitation
  - Luciferase
- QUANTIFICATION AND STATISTICAL ANALYSIS

SUPPLEMENTAL INFORMATION

Supplemental information can be found online at https://doi.org/10.1016/j.isci.2024.109917.

ACKNOWLEDGMENTS

This work was supported by National Key R&D Program of China (2022YFA1604503, 2022YFA1104302), and Foundation of State Key Laboratory of Space Medicine, China Astronaut Research and Training Center (SMFA20A01). We thank Yinghui Li, director of the State Key Laboratory of Space Medicine, for her support of this work.

AUTHOR CONTRIBUTIONS

LQ, BS and XL interpreted the data and designed the structure of the article. SZ, SC, CZ, WZ, NY and SZ provided materials. KL analyzed the data. YZ and GJ carried out the experiments and wrote the article with input from all other authors. All authors read and approved the final article.

DECLARATION OF INTERESTS

The authors declare no competing interests.

Received: January 22, 2024
Revised: March 6, 2024
Accepted: May 3, 2024
Published: May 7, 2024

REFERENCES

1. Avital, A., Goshen, I., Kamsler, A., Segal, M., Iverfeldt, K., Richter-Levin, G., and Yirmiya, R. (2003). Impaired interleukin-1 signaling is associated with deficits in hippocampal memory processes and neural plasticity. Hippocampus *13*, 826–834.
2. Barisano, G., Sepehrband, F., Collins, H.R., Jillings, S., Jeurissen, B., Taylor, J.A., Schoenmaekers, C., De Laet, C., Rukavishnikov, I., Nosikova, I., et al. (2022). The effect of prolonged spaceflight on cerebrospinal fluid and perivascular spaces of astronauts and cosmonauts. Proc. Natl. Acad. Sci. USA *119*. e2120439119.
3. Blaschke, R.J., Hahurij, N.D., Kuijper, S., Just, S., Wisse, L.J., Deissler, K., Maxelon, T., Anastassiadis, K., Spitzer, J., Hardt, S.E., et al. (2007). Targeted mutation reveals essential functions of the homeodomain transcription factor Shox2 in sinoatrial and pacemaking development. Circulation *115*, 1830–1838.
4. Braatz, C., Komes, M.P., Ravichandran, K.A., de Fragas, M.G., Griep, A., Schwartz, S., McManus, R.M., and Heneka, M.T. (2023). NLRP3-directed antisense oligonucleotides reduce microglial immunoactivities in vitro. J. Neurochem. https://doi.org/10.1111/jnc.15778.
5. Castro-Hernández, R., Berulava, T., Metelova, M., Epple, R., Peña Centeno, T., Richter, J., Kaurani, L., Pradhan, R., Sakib, M.S., Burkhardt, S., et al. (2023). Conserved reduction of m(6)A RNA modifications during aging and neurodegeneration is linked to changes in synaptic transcripts. Proc. Natl. Acad. Sci. USA *120*. e2204933120.
6. Chen, Z., and Zhou, J. (2024). METTL3 promotes cellular senescence of colorectal cancer via modulation of CDKN2B transcription and mRNA stability. Oncogene *43*, 976–991. https://doi.org/10.1038/s41388-41024-02956-y.
7. Costello, D.A., Watson, M.B., Cowley, T.R., Murphy, N., Murphy Royal, C., Garlanda, C., and Lynch, M.A. (2011). Interleukin-1alpha and HMGB1 mediate hippocampal dysfunction in SIGIRR-deficient mice. J. Neurosci. *31*, 3871–3879.
8. D'Hooge, R., and De Deyn, P.P. (2001). Applications of the Morris water maze in the study of learning and memory. Brain Res. Brain Res. Rev. *36*, 60–90.
9. da Silveira, W.A., Fazelinia, H., Rosenthal, S.B., Laiakis, E.C., Kim, M.S., Meydan, C., Kidane, Y., Rathi, K.S., Smith, S.M., Stear, B., et al. (2020). Comprehensive Multi-omics Analysis Reveals Mitochondrial Stress as a Central Biological Hub for Spaceflight Impact. Cell *183*, 1185–1201.e20.
10. Dougherty, K.J., Zagoraiou, L., Satoh, D., Rozani, I., Doobar, S., Arber, S., Jessell, T.M., and Kiehn, O. (2013). Locomotor rhythm generation linked to the output of spinal shox2 excitatory interneurons. Neuron *80*, 920–933.
11. Gaikwad, S., Senapati, S., Haque, M.A., and Kayed, R. (2024). Senescence, brain inflammation, and oligomeric tau drive cognitive decline in Alzheimer's disease: Evidence from clinical and preclinical studies. Alzheimers Dement. *20*, 709–727.
12. Garrett-Bakelman, F.E., Darshi, M., Green, S.J., Gur, R.C., Lin, L., Macias, B.R., McKenna, M.J., Meydan, C., Mishra, T., Nasrini, J., et al. (2019). The NASA Twins Study: A multidimensional analysis of a year-long human spaceflight. Science *364*, eaau8650.
13. Gong, X., Huang, M., and Chen, L. (2024). NRF1 mitigates motor dysfunction and dopamine neuron degeneration in mice with Parkinson's disease by promoting GLRX m(6)A methylation through upregulation of METTL3 transcription. CNS Neurosci. Ther. *30*, e14441. https://doi.org/10.1111/cns.14441.
14. Gonzales, M.M., Garbarino, V.R., Pollet, E., Palavicini, J.P., Kellogg, D.L., Jr., Kraig, E., and Orr, M.E. (2022). Biological aging processes underlying cognitive decline and neurodegenerative disease. J. Clin. Invest. *132*, e158453.
15. Goshen, I., Kreisel, T., Ounallah-Saad, H., Renbaum, P., Zalzstein, Y., Ben-Hur, T., Levy-Lahad, E., and Yirmiya, R. (2007). A dual role for interleukin-1 in hippocampal-dependent memory processes. Psychoneuroendocrinology *32*, 1106–1115.
16. Guerrero, A., De Strooper, B., and Arancibia-Cárcamo, I.L. (2021). Cellular senescence at the crossroads of inflammation and Alzheimer's disease. Trends Neurosci. *44*, 714–727.
17. Gulen, M.F., Samson, N., Keller, A., Schwabenland, M., Liu, C., Glück, S., Thacker, V.V., Favre, L., Mangeat, B., Kroese, L.J., et al. (2023). cGAS-STING drives ageing-related inflammation and neurodegeneration. Nature *620*, 374–380.
18. Ha, N.T., and Dougherty, K.J. (2018). Spinal Shox2 interneuron interconnectivity related to function and development. Elife *7*, e42519.
19. Heneka, M.T., Carson, M.J., El Khoury, J., Landreth, G.E., Brosseron, F., Feinstein, D.L., Jacobs, A.H., Wyss-Coray, T., Vitorica, J., Ransohoff, R.M., et al. (2015). Neuroinflammation in Alzheimer's disease. Lancet Neurol. *14*, 388–405.
20. Holley, J.M., Stanbouly, S., Pecaut, M.J., Willey, J.S., Delp, M., and Mao, X.W. (2022). Characterization of gene expression profiles in the mouse brain after 35 days of spaceflight mission. NPJ microgravity *8*, 35.
21. Huang, H., Song, R., Wong, J.J.L., Anggono, V., and Widagdo, J. (2023). The N6-methyladenosine RNA landscape in the aged mouse hippocampus. Aging Cell *22*, e13755.
22. Ji, G., Chang, H., Yang, M., Chen, H., Wang, T., Liu, X., Lv, K., Li, Y., Song, B., and Qu, L. (2022). The mitochondrial proteomic changes of rat hippocampus induced by 28-day simulated microgravity. PLoS One *17*, e0265108.
23. Kaneko, M., Stellwagen, D., Malenka, R.C., and Stryker, M.P. (2008). Tumor necrosis factor-alpha mediates one component of competitive, experience-dependent plasticity in developing visual cortex. Neuron *58*, 673–680.
24. Kokhan, V.S., Matveeva, M.I., Mukhametov, A., and Shtemberg, A.S. (2016). Risk of defeats in the central nervous system during deep space missions. Neurosci. Biobehav. Rev. *71*, 621–632.
25. Krukowski, K., Grue, K., Becker, M., Elizarraras, E., Frias, E.S., Halvorsen, A., Koenig-Zanoff, M., Frattini, V., Nimmagadda, H., Feng, X., et al. (2021). The impact of deep space radiation on cognitive performance: From biological sex to biomarkers to countermeasures. Sci. Adv. *7*, eabg6702.
26. Lecca, D., Jung, Y.J., Scerba, M.T., Hwang, I., Kim, Y.K., Kim, S., Modrow, S., Tweedie, D., Hsueh, S.C., Liu, D., et al. (2022). Role of chronic neuroinflammation in neuroplasticity and cognitive function: A hypothesis. Alzheimers Dement. *18*, 2327–2340.
27. Lissner, L.J., Wartchow, K.M., Toniazzo, A.P., Gonçalves, C.A., and Rodrigues, L. (2021). Object recognition and Morris water maze to detect cognitive impairment from mild hippocampal damage in rats: A reflection based on the literature and experience. Pharmacol. Biochem. Behav. *210*, 173273.
28. Liu, P., Li, F., Lin, J., Fukumoto, T., Nacarelli, T., Hao, X., Kossenkov, A.V., Simon, M.C., and Zhang, R. (2021). m(6)A-independent genome-wide METTL3 and METTL14 redistribution drives the senescence-associated secretory phenotype. Nat. Cell Biol. *23*, 355–365.
29. Martinez De La Cruz, B., Markus, R., Malla, S., Haig, M.I., Gell, C., Sang, F., Bellows, E., Sherif, M.A., McLean, D., Lourdusamy, A., et al. (2021). Modifying the m(6)A brain methylome by ALKBH5-mediated demethylation: a new contender for synaptic tagging. Mol. Psychiatry *26*, 7141–7153.
30. Merkurjev, D., Hong, W.T., Iida, K., Oomoto, I., Goldie, B.J., Yamaguti, H., Ohara, T., Kawaguchi, S.Y., Hirano, T., Martin, K.C., et al. (2018). Synaptic N(6)-methyladenosine (m(6)A) epitranscriptome reveals functional partitioning of localized transcripts. Nat. Neurosci. *21*, 1004–1014.
31. Olivetti, P.R., Maheshwari, A., and Noebels, J.L. (2014). Neonatal estradiol stimulation prevents epilepsy in Arx model of X-linked infantile spasms syndrome. Sci. Transl. Med. *6*, 220ra12.
32. Parihar, V.K., Allen, B., Tran, K.K., Macaraeg, T.G., Chu, E.M., Kwok, S.F., Chmielewski, N.N., Craver, B.M., Baulch, J.E., Acharya, M.M., et al. (2015). What happens to your brain on the way to Mars. Sci. Adv. *1*, e1400256.
33. Preitner, N., Quan, J., Li, X., Nielsen, F.C., and Flanagan, J.G. (2016). IMP2 axonal localization, RNA interactome, and function in the development of axon trajectories. Development (Cambridge, England) *143*, 2753–2759.
34. Qiong, W., Yong-Liang, Z., Ying-Hui, L., Shan-Guang, C., Jiang-Hui, G., Yi-Xi, C., Ning, J., and Xin-Min, L. (2016). The memory enhancement effect of Kai Xin San on cognitive deficit induced by simulated

weightlessness in rats. J. Ethnopharmacol. *187*, 9–16.
35. Scavone, A., Capilupo, D., Mazzocchi, N., Crespi, A., Zoia, S., Campostrini, G., Bucchi, A., Milanesi, R., Baruscotti, M., Benedetti, S., et al. (2013). Embryonic stem cell-derived CD166+ precursors develop into fully functional sinoatrial-like cells. Circ. Res. *113*, 389–398.
36. Schmid, A.W., Lynch, M.A., and Herron, C.E. (2009). The effects of IL-1 receptor antagonist on beta amyloid mediated depression of LTP in the rat CA1 in vivo. Hippocampus *19*, 670–676.
37. Scott, A., Hasegawa, H., Sakurai, K., Yaron, A., Cobb, J., and Wang, F. (2011). Transcription factor short stature homeobox 2 is required for proper development of tropomyosin-related kinase B-expressing mechanosensory neurons. J. Neurosci. *31*, 6741–6749.
38. Shi, H., Zhang, X., Weng, Y.L., Lu, Z., Liu, Y., Lu, Z., Li, J., Hao, P., Zhang, Y., Zhang, F., et al. (2018). m(6)A facilitates hippocampus-dependent learning and memory through YTHDF1. Nature *563*, 249–253.
39. Stellwagen, D., Beattie, E.C., Seo, J.Y., and Malenka, R.C. (2005). Differential regulation of AMPA receptor and GABA receptor trafficking by tumor necrosis factor-alpha. J. Neurosci. *25*, 3219–3228.
40. Strollo, F., and Vernikos, J. (2021). Aging-like metabolic and adrenal changes in microgravity: State of the art in preparation for Mars. Neurosci. Biobehav. Rev. *126*, 236–242.
41. Tzeng, T.C., Hasegawa, Y., Iguchi, R., Cheung, A., Caffrey, D.R., Thatcher, E.J., Mao, W., Germain, G., Tamburro, N.D., Okabe, S., et al. (2018). Inflammasome-derived cytokine IL18 suppresses amyloid-induced seizures in Alzheimer-prone mice. Proc. Natl. Acad. Sci. USA *115*, 9002–9007.
42. Viatchenko-Karpinski, V., Kong, L., and Weng, H.R. (2022). Activation of microglial GPR109A alleviates thermal hyperalgesia in female lupus mice by suppressing IL-18 and glutamatergic synaptic activity. Glia *70*, 634–649.
43. Wang, J., Yan, S., Lu, H., Wang, S., and Xu, D. (2019). METTL3 Attenuates LPS-Induced Inflammatory Response in Macrophages via NF-κB Signaling Pathway. Mediators Inflamm. *2019*, 3120391.
44. Williams, J.A., Burgess, S., Suckling, J., Lalousis, P.A., Batool, F., Griffiths, S.L., Palmer, E., Karwath, A., Barsky, A., Gkoutos, G.V., et al. (2022). Inflammation and Brain Structure in Schizophrenia and Other Neuropsychiatric Disorders: A Mendelian Randomization Study. JAMA Psychiatr. *79*, 498–507.
45. Xiao, K., Liu, P., Yan, P., Liu, Y., Song, L., Liu, Y., and Xie, L. (2022). N6-methyladenosine reader YTH N6-methyladenosine RNA binding protein 3 or insulin like growth factor 2 mRNA binding protein 2 knockdown protects human bronchial epithelial cells from hypoxia/reoxygenation injury by inactivating p38 MAPK, AKT, ERK1/2, and NF-κB pathways. Bioengineered *13*, 11973–11986.
46. Yang, J., Liu, J., Liu, J., Li, W., Li, X., He, Y., and Ye, L. (2014). Genetic association study with metabolic syndrome and metabolic-related traits in a cross-sectional sample and a 10-year longitudinal sample of chinese elderly population. PLoS One *9*, e100548.
47. Yin, H., Ju, Z., Zheng, M., Zhang, X., Zuo, W., Wang, Y., Ding, X., Zhang, X., Peng, Y., Li, J., et al. (2023). Loss of the m6A methyltransferase METTL3 in monocyte-derived macrophages ameliorates Alzheimer's disease pathology in mice. PLoS Biol. *21*, e3002017.
48. Yu, D., Febbo, I.G., Maroteaux, M.J., Wang, H., Song, Y., Han, X., Sun, C., Meyer, E.E., Rowe, S., Chen, Y., et al. (2021). The Transcription Factor Shox2 Shapes Neuron Firing Properties and Suppresses Seizures by Regulation of Key Ion Channels in Thalamocortical Neurons. Cereb. Cortex *31*, 3194–3212.
49. Zhang, H., Chen, C., Liu, Y., Ren, L., Qi, J., Yang, Y., Chen, W., Yao, Y., Cai, X., Liu, Z., et al. (2022). NRF-2/HO-1 Pathway-Mediated SHOX2 Activation Is a Key Switch for Heart Rate Acceleration by Yixin-Fumai Granules. Oxid. Med. Cell. Longev. *2022*, 8488269.
50. Zhang, H., Chen, C., Liu, Y., Chen, W., Qi, J., Xu, Y., Ren, L., Yang, G., Min, D., Liu, Z., et al. (2023). D-galactose causes sinoatrial node dysfunction: from phenotype to mechanism. Aging *15*, 12551–12569.
51. Zhang, X., Chu, X., Chen, L., Fu, J., Wang, S., Song, J., Kan, G., Jiang, W., He, G., Chen, X., and Li, W. (2019). Simulated weightlessness procedure, head-down bed rest impairs adult neurogenesis in the hippocampus of rhesus macaque. Mol. Brain *12*, 46.
52. Zhang, Y., Wang, Q., Chen, H., Liu, X., Lv, K., Wang, T., Wang, Y., Ji, G., Cao, H., Kan, G., et al. (2018). Involvement of Cholinergic Dysfunction and Oxidative Damage in the Effects of Simulated Weightlessness on Learning and Memory in Rats. BioMed Res. Int. *2018*, 2547532.
53. Zhao, F., Xu, Y., Gao, S., Qin, L., Austria, Q., Siedlak, S.L., Pajdzik, K., Dai, Q., He, C., Wang, W., et al. (2021). METTL3-dependent RNA m(6)A dysregulation contributes to neurodegeneration in Alzheimer's disease through aberrant cell cycle events. Mol. Neurodegener. *16*, 70.
54. Zong, X., Zhao, J., Wang, H., Lu, Z., Wang, F., Du, H., and Wang, Y. (2019). Mettl3 Deficiency Sustains Long-Chain Fatty Acid Absorption through Suppressing Traf6-Dependent Inflammation Response. J. Immunol. *202*, 567–578.

STAR★METHODS

KEY RESOURCES TABLE

REAGENT or RESOURCE	SOURCE	IDENTIFIER
Deposited data		
Raw data	the CNSA of CNGBdb (https://db.cngb.org/cnsa/)	CNGBdb: CNP0005438
Experimental models: Cell lines		
HT 22 cell line	Procell	Cat# CL-0697
Experimental models: Organisms/strains		
Mouse: eight-week-old male C57BL/6J mice	Sibeifu Animal Company	N/A
Antibodies		
m6A antibody	Synaptic Systems	Cat# 202 003; RRID:AB_2279214
Rabbit (DA1E) mAb IgG XP® Isotype Control	Cell Signaling Technology	Cat# 2729S; RRID:AB_2150103
Alpha Tubulin Monoclonal antibody	Proteintech	Cat# 66031-1-Ig; RRID:AB_11042766
IMP2 (D4R2F) Rabbit mAb	Cell Signaling Technology	Cat# 14672; RRID:AB_2798563
Mouse monoclonal [1D1] to SHOX2	Abcam	Cat# ab55740; RRID:AB_945451
PSD95 (D27E11) XP® Rabbit mAb	Cell Signaling Technology	Cat# 3450S; RRID:AB_11066201
BDNF Antibody	Cell Signaling Technology	Cat# 47808; RRID:AB_2894709
CREB (48H2) Rabbit mAb	Cell Signaling Technology	Cat# 9197; RRID:AB_331277
Phospho-CREB (Ser133) (87G3) Rabbit mAb	Cell Signaling Technology	Cat# 9198; RRID:AB_2561044
METTL3 (E3F2A) Rabbit mAb	Cell Signaling Technology	Cat# 86132; RRID:AB_2800072
METTL14 (D8K8W) Rabbit mAb	Cell Signaling Technology	Cat# 51104; RRID:AB_2799383
WTAP Antibody	Cell Signaling Technology	Cat# 56501; RRID:AB_2799512
ALKBH5 (E3F6E) Rabbit mAb	Cell Signaling Technology	Cat# 49015; RRID:AB_11466886
FTO (D2V1I) Rabbit mAb	Cell Signaling Technology	Cat# 45980; RRID:AB_2799294
CACNA1G Polyclonal antibody	Proteintech	Cat# 17821-1-AP; RRID:AB_2878446
HRP-Goat Anti-Rabbit IgG(H + L)	Huaxingbio	Cat# HX2031; RRID:AB_2475959
HRP-Goat Anti-Mouse IgG(H + L)	Huaxingbio	Cat# HX2032; RRID:AB_2795639
Chemicals, peptides, and recombinant proteins		
Lipofectamine™3000	Invitrogen	Cat# 3000075
Lipofectamine™ RNAiMAX	Invitrogen	Cat# 13778150
protease inhibitors	Huaxingbio	Cat# HX1863
phosphatase inhibitors	Huaxingbio	Cat# HX1864
RNase inhibitor	ThermoFisher	Cat# 87785
Magna RIP RNA-Binding Protein Immunoprecipitation Kit	Millipore	Cat# 17-701
PrimeScript™ RT reagent Kit	Takara.	Cat# RR037A
Senescence β-Galactosidase Staining Kit	Beyotime	Cat# C0602
Dual-Luciferase Reporter Assay System	Promega	Cat# E1960
TRIzol Reagent	Ambion	Cat# 10296028
Recombinant DNA		
pECMV-3×FLAG-N	Fenghuishengwu	N/A
pECMV-Igf2bp2	Fenghuishengwu	N/A
pcDNA3.1	Fenghuishengwu	N/A
pcDNA3.1-Shox2	Fenghuishengwu	N/A
pGL3	Fenghuishengwu	N/A
pGL3-Shox2-3′UTR	Fenghuishengwu	N/A

(*Continued on next page*)

Continued

REAGENT or RESOURCE	SOURCE	IDENTIFIER
Oligonucleotides		
Primers used in this study, see Excel S1	This paper	N/A
Si-NC Sence: 5′UCUCCGAACGUGUCACGUTT-3′ Antisence: 5′CGUGACACGUUCGGAGAATT-3′	GenePharma	N/A
si-Shox2 Sence: 5′GCUUUCAUGCGCGAGGAAUTT-3′ Antisence: 5′UUCCUCGCGCAUGAAAGCTT-3′	GenePharma	N/A
si-Igf2bp2 Sence: 5′CCGUUAACCAACAAGCCAATT-3′ Antisence: 5′UUGGCUUGUUGGUUAACGGTT-3′	GenePharma	N/A
Bacterial and virus strains		
HBAAV2/9-vector	HANBIO	N/A
HBAAV2/9-IGF2BP2	HANBIO	N/A
HBAAV2/9-SHOX2	HANBIO	N/A
Software and algorithms		
GraphPad Prism 8	GraphPad	N/A
SPSS 22.0	IBM	N/A
ImageJ	NIH	N/A

RESOURCE AVAILABILITY

Lead contact

Further information and requests for resources and reagents should be directed to and will be fulfilled by the lead contact, Lina Qu (linaqu@263.net).

Materials availability

This study did not generate new unique reagents.

Data and code availability

- Raw data of this study have been deposited in the CNSA. CNGBdb: CNP0005438, The DOI and accession number are listed in the key resources table. All other data reported in this paper will be shared by the lead contact upon request.
- This paper does not report original code.
- Any additional information required to reanalyze the data reported in this paper is available from the lead contact upon request.

EXPERIMENTAL MODEL AND SUBJECT DETAILS

HT22 cells (Procell, Wuhan, China) were cultured in DMEM medium (Gibco) with 10% FBS (Gibco), at 37°C with 5% CO2.

Eight-week-old male C57BL/6N mice used in this study were sourced from Beijing Sibeifu Animal Company [Animal license number: SCXK (Beijing) 2012–0001]. The animals were housed in a humidity controlled (60% ± 10%) room with a temperature of 24°C ± 1°C and a 12-h light/12-h dark cycle (lights-on from 8:00 to 20:00). All experimental procedures involving the mice were approved by the Animal Care and Use Committee of the China Astronaut Research and Training Center (reference number: ACC-IACUC-2022-016). All animal studies were performed in accordance with the approved guidelines for the use and care of live animals.

METHOD DETAILS

Tail suspension

The mice performed tail suspension after adapted for one week. The mice were placed in the cage individually, with tails tied with medical tape and hung by the chain on the top of the cage. This method can mimic weightlessness, allowing mice to maintain their hind legs at about a 30° angle from the ground for 42 days. The mice were allowed free access to water and food.

Morris water maze test

The Morris water maze test was divided into two phases: training phase and space exploration test phase. The five days of training, the animals were lowered into the water twice a day from different quadrants, with platforms hidden 1.5 cm below the surface. The space exploration test was carried out on the sixth day while the platform was dismantled. The data were analyzed after the experiment.

Novel object recognition (NOR)/object location recognition test (OLRT)

Before the start of the experiment, the mice went through a familiarization period, and the mice were placed in the test box for 10 min to acclimatize for 1 day. Two identical objects were placed symmetrically on one side of the test chamber, the mice explored for 5 min for familiarity stage. After 30 min, one object was replaced by a different object (novel object recognition), or moved to the opposite position (object location recognition test). The memory ability of animals was evaluated by resolution index (DI). The calculation formula is DI = (TN-TF)/(TN + TF) × 100%. TN (new) and TF (familiar) represent the exploration time of a new object or object in a new location and the exploration time of an object in a familiar location, respectively.

Stereotaxic injection into the hippocampus

Mice were anesthetized with isoflurane and immobilized on the operating table. An incision was made on the scalp to expose the skull, and the target region coordinates were CA1 (bregma 2.3mm, L/R 1.8mm, V 2.0mm). The HBAAV2/9-vector, HBAAV2/9-IGF2BP2 and HBAAV2/9-SHOX2 were injected slowly with a microinjector and allowed to stand for 5 min to ensure diffusion and reduce reflux. The incision was closed after injection.

Western blotting analysis

Tissues and cells homogenized with protein cleavage buffer containing protease inhibitor (huaxingbio, China) lysed for 30 min. After 15 min of centrifugation at 13000*g*, 4°C, the supernatant was quantified using bicinchoninic acid (BCA) method (Thermo, USA). The sample was boiled at 100°C with SDS buffer for 5 min. The proteins were isolated by 7.5% or 10% SDS/PAGE and transferred onto PVDF membrane (Merck Millipore, Germany) and then closed at room temperature for 1 h with 5% skim milk of Tris-Buffered Saline Tween (TBST) (Solarbio, China). The membrane was combined with primary antibody PSD95 (1:1000, CST), CREB/p-CREB (1:1000, CST), METTL3 (1:1000, CST), METTL14 (1:1000, CST), WTAP (1:1000, CST), FTO (1:1000, CST), ALKBH5 (1:1000, CST), IGF2BP2 (1:1000, CST), Shox2 (1:500, Abcam), Cacna1g (1:500, proteintech), α-tubulin (1:2000, proteintech), and β-actin (1:2000, proteintech) were incubated at 4°C overnight, and then incubated with enzyme-labeled secondary antibody at room temperature for 1 h. Protein bands were displayed using ECL kit (Millpore). The ImageJ software is used to analyze the gray value with density.

Nissl's staining

After dewaxed the paraffin sections of each group, the xylene was rehydrated with graded ethanol (70%, 95% and 100%) and then rehydrated with distilled water. The staining was performed with the Nissl staining kit (Jiancheng Biology, China). The integrated optical density of Nissl in each group was quantitatively analyzed by using microscope imaging and ImageJ software.

RT-PCR and RT-qPCR

TRIzol reagent (Invitrogen, USA) was used for tissues or cells RNA extraction. RNA was quantified using Nanodrop 2000. Reverse transcription and qRT-PCR reactions were performed using PrimeScriptTM RT kit (TAKARA, China) and TB GREEN SuperMix (TAKARA, China) to analyze mRNA expression. The mRNA levels were normalized by GAPDH. The primer sequences are listed in Supplement Excel 1.

Vector construction and cell transfection

IGF2BP2 and Shox2 overexpressed empty plasmid were constructed Fenghui Biotech. For the mutant version of Shox2, the sequence of "AGACC", "AGACT" or "GGACA" was replaced with "AGCCC", "AGCCT" or "GGCCA", respectively, using the KOD plus (Vazyme, Nanjing, China).

The transfection of siRNAs and plasmids was performed using the RNAimax (Invitrogen) and Lipofectamine 3000 kit (Invitrogen) according to the manufacturer's instructions. The siRNA sequences are listed in key resources table.

D-gal treat cells

The cells were treated with 100 mM D-gal and 0 mM was used as the control group, and HT22 cells were collected 48 h later for follow-up experiments.

Senescence-associated β-galactosidase stain (SA-β-gal stain)

Frozen sections or cells were washed three times with PBS and fixed at room temperature with 2% formaldehyde and 0.2% glutaraldehyde for 15 min. After washing with PBS, the sections or cells were incubated with 1 mL β-galactosidase working solution (10 μL of the enzyme A plus 10 μL of the enzyme B plus 930 μL of the enzyme C plus 50 μL of the X-Gal solution) at 37 °C overnight. The staining was performed with the

Senescence β-Galactosidase Staining Kit (Beyotime Biology, China). Under a standard optical microscope, the PBS replacement staining solution was observed and captured on camera. The intensity of SA-β-Gal-positive cells or area was calculated using ImageJ.

Immunohistochemistry (IHC)

The brain paraffin sections were fixed in 4% paraformaldehyde solution for 24 h. After antigen repair, gradient dehydration and 5% serum blocking, incubated with m6A antibody (1:200) at 4°C overnight. The stained slides were assessed with integrated optical density (IOD) using ImageJ software.

MeRIP-qPCR

The total RNA was extracted using Trizol. 50 ng of the total RNA was saved as a standardized control of input. After fragmentation and denaturation, RNase inhibitor was added and 3 μg RNA was incubated with an anti-m6A antibody(Synaptic Systems, Germany) together with protein A/G magnetic beads (MCE, China) in immunoprecipitation buffer (150 mM NaCl, 10 mM Tris-HCl, pH 7.4, 0.1% NP-40) at 4°C overnight. Eluted three times with elution buffer (5 mM Tris-HCL pH 7.5, 1 mM EDTA pH 8.0, 0.05% SDS, 20 mg/mL Proteinase K) and used for RT-qPCR.

MeRIP-seq data analysis

Raw data (raw reads) of fastq format were firstly processed using the Trimmomatic software. Clean data (clean reads) were obtained by removing reads containing adapter, reads containing ploy-N and low-quality reads from raw data. Use the SortMeRNA software for ribosomal RNA reads removal. After discarded the rRNA reads, the remain clean reads were mapped to the reference genome using HISAT2 with default parameters. Unique reads with high mapping quality were retained. To accessing the quality of methylated RNA immunoprecipitation sequencing data. Used the Guitar R package and deeptools software for evaluation of m6A-seq data quality. The m6A-enriched peaks in each m6A immunoprecipitation sample were identified by MeTDiff peak calling software with the corresponding input sample serving as control. The differential peaks were detected by MeTDiff with parameter ('FRAGMENT_LENGTH = 200, PEAK_CUTOFF_PVALUE = 0.01, DIFF_PEAK_CUTOFF_FDR = 0.05, PEAK_CUTOFF_FDR = 0.05'), after which, differential peaks were annotated by ChIPseeker. GO enrichment and KEGG pathway enrichment analysis of peaks and differential peaks were performed respectively using R based on the hypergeometric distribution.

RNA immunoprecipitation

RIP experiments were performed with a Magna RIP RNA-Binding Protein Immunoprecipitation Kit (Millipore, Billerica, MA, USA) according to the manufacturer's instructions. Briefly, protein A/G magnetic beads conjugated with rabbit immunoglobulin G, IGF2BP2 (CST, USA) antibody were incubated with cell lysates supplemented with RNase inhibitor at 4°C overnight. Co-precipitated RNA was detected by RT-qPCR.

Luciferase

HT22 cells were seeded in a 48-well plate and transfected with the Shox2-3′-UTR of wild type and the Shox2-m6A site mutant plasmids using lipo3000 (Invitrogen, USA). After 24 h, the cells were lysed for 20 min then transferred to a white opaque 96-well plate. Luciferase Reagent and Stop & Glo reagent solution (Promega, Madison, Wisconsin, USA) were configured and tested on the machine. The data were analyzed by the ratio of the luciferase detection value of firefly to the luciferase detection value of renilla luciferase.

QUANTIFICATION AND STATISTICAL ANALYSIS

The t test was applied for comparisons between two groups, and one-way analysis of variance (ANOVA) was used for multi-groups. All data were presented as the mean ± standard error of mean (SEM) and analyzed using the GraphPad Prism 8.0 software. $p < 0.05$ was considered statistically significant. The use of an asterisk to indicate p values is statistically significant. *$p < 0.05$, **$p < 0.01$, ***$p < 0.001$. Statistical details for each experiment are included in the figures and figure legends.